Received: 27 May 2016 | Revised: 18 October 2016 | Accepted: 13 November 2016

DOI 10.1002/aoc.3703

WILEY Applied Organometallic Chemistry

FULL PAPER

Metallated porphyrin noncovalent interaction with reduced graphene oxide-modified electrode for amperometric detection of environmental pollutant hydrazine

Subramanian Sakthinathan[1] | Subbiramaniyan Kubendhiran[1] | Shen-Ming Chen[1,2] | Mani Govindasamy[1] | Fahad M.A. Al-Hemaid[2] | M. Ajmal Ali[2] | P. Tamizhdurai[3] | S. Sivasanker[3]

[1] Electroanalysis and Bioelectrochemistry Lab, Department of Chemical Engineering and Biotechnology, National Taipei University of Technology, No. 1, Section 3, Chung-Hsiao East Road, Taipei 106, Taiwan

[2] Department of Botany and Microbiology, College of Science, King Saud University, Riyadh 11451, Saudi Arabia

[3] National Centre for Catalysis Research (NCCR), Indian Institute of Technology, Chennai –600036, India

Correspondence
Shen-Ming Chen, Electroanalysis and Bioelectrochemistry Lab, Department of Chemical Engineering and Biotechnology, National Taipei University of Technology, No. 1, Section 3, Chung-Hsiao East Road, Taipei 106, Taiwan (ROC).
Email: smchen78@ms15.hinet.net
S. Sivasanker, National Centre for Catalysis Research (NCCR), Indian Institute of Technology, Chennai–600036, India.
Email: ssivasanker@iitm.ac.in

A reduced graphene oxide/platinum(II) tetraphenylporphyrin nanocomposite (RGO/Pt-TPP)-modified glassy carbon electrode was developed for the selective detection of hydrazine. The RGO/Pt-TPP nanocomposite was successfully prepared via noncovalent π–π stacking interaction. The prepared nanocomposite was characterized using nuclear magnetic resonance, electrochemical impedance, ultraviolet–visible and Raman spectroscopies, scanning electron microscopy and X-ray diffraction. The electrochemical detection of hydrazine was performed via cyclic voltammetry and amperometry. The RGO/Pt-TPP nanocomposite exhibited good electrocatalytic activity towards detection of hydrazine with low overpotential and high oxidation peak current. The fabricated sensor exhibited a wide linear range from 13 nM to 232 μM and a detection limit of 5 nM. In addition, the fabricated sensor selectively detected hydrazine even in the presence of 500-fold excess of common interfering ions. The fabricated electrode exhibited good sensitivity, stability, repeatability and reproducibility. In addition, the practical applicability of the sensor was evaluated in various water samples with acceptable recoveries.

KEYWORDS

amperometric technique, electrocatalysis, hydrazine, platinum tetraphenylporphyrin, pollutant sensor, reduced graphene oxide, selectivity, sensitivity

1 | INTRODUCTION

Hydrazine (N_2H_4) is a simple inorganic molecule with a molecular weight of 32.04 g mol^{-1} and its derivatives are well known due to their extensive applications in various fields, such as corrosion inhibitors, oxygen scavengers, rocket propellants, photographic chemicals, plastic blowing agents, dyes, explosives and pesticides.[1–5] However, hydrazine and its derivatives are biologically toxic and environmental pollutants; they can be easily absorbed via oral, skin and respiratory routes. Hence, hydrazine is highly toxic to humans and animals, and it causes several health effects.[6] In addition, the World Health Organization has classified the hydrazine as a B2 group human carcinogenic agent. Therefore, sensitive and selective detection of hydrazine is very important.[7,8]

Numerous analytical methods have been developed for the detection of hydrazine, such as spectrophotometric methods,[9] high-performance liquid chromatography,[10] titrimetry,[11] flow injection analysis,[12] gas chromatography,[13] potentiometry,[14] colorimetric determination[15] and capillary electrophoresis.[16] However, these kinds of methods involve time-consuming processes and require tedious protocols. On the contrary, electrochemical methods are facile, sensitive and selective compared to other traditional analytical methods.[17–19] Hydrazine is electrochemically active on glassy carbon electrodes (GCEs), screen-printed carbon electrodes and graphite electrodes. Unfortunately, these

unmodified electrodes have some drawbacks such as high overpotential and low sensitivity. Therefore, a suitable modified electrode is required to resolve these problems.

Graphene as a two-dimensional, one-atom-thick planar sheet comprising an sp^2 carbon network has attracted attention because of its extraordinary electronic properties. Due to the unique properties of graphene, it is a promising material for potential applications in a variety of fields, for instance in nanoelectronics, supercapacitors, catalysis, batteries, drug delivery and sensors. Nowadays, the chemical conversion of graphite to graphene oxide (GO) is one of the most advanced methods to achieve single-layer graphene. However, reduced graphene oxide (RGO) is more electron conductive than GO (*ca* 225.3 S m^{-1}).[20] RGO can be prepared using different kinds of methods such as thermal, chemical and electrochemical methods.[21] The electrochemical method is a good alternative to chemical and thermal methods due to its simplicity, low cost and environmental friendliness. In addition, the electrochemical preparation of RGO has advantages in terms of control of film thickness and highly stable product.[22,23]

Porphyrins are a class of macrocyclic conjugated organic molecules, having four pyrrole rings connected with methane bridges. Hence, porphyrin metallated by transition metals promotes the aromatic character.[24–26] Metallated porphyrin has been used as an electrocatalyst for oxidation and reduction reactions.[27,28] The reactivity of a metalloporphyrin depends upon the central metal ions and the substituents on the porphyrin ring. Platinum is one of the most attractive metals due to its outstanding electrocatalytic activity. Hence, platinum has been metallated into the porphyrin macromolecule to form platinum(II) tetraphenylporphyrin (Pt-TPP). Pt-TPP has been investigated as an oxygen sensor,[29,30] photosensitizer,[31,32] antitumor agent[33] and molecular conductor.[34,35] Moreover, the highly emissive triplet states and extended π-ring system of Pt–porphyrin are conducive for use in sensing and biological imaging applications.

The properties of metalloporphyrin have been extensively studied by covalent and noncovalent functionalization with graphene materials. However, the noncovalent functionalization of metallated porphyrin has advantages over covalent functionalization due to its being simple, convenient, avoiding destruction and preserving the unique properties.[36–38] The main objective of the work presented here was to prepare Pt-TPP molecules decorated with RGO through noncovalent π–π stacking interaction. Electrochemical reduction was used to increase the interaction between Pt-TPP and RGO. Hence, the as-prepared RGO/Pt-TPP nanocomposite exhibited a high electrocatalytic activity towards the oxidation of hydrazine, with a lower oxidation potential (−0.25 V) and wider linear concentration range (13 nM to 232 μM) than those of other reported hydrazine sensors.

2 | EXPERIMENTAL

2.1 | Materials and methods

Purified graphite powder (1–2 μm), pyrrole, propionic acid, benzaldehyde, platinum(II) chloride, potassium ferricyanide, potassium ferrocyanide and other chemicals were obtained from Sigma Aldrich. Hydrochloric acid, sulfuric acid and hydrazine monohydrate were purchased from Merck. All the purchased chemicals were of analytical grade and used without any purification. Phosphate-buffered saline (PBS; pH = 7) was prepared using 0.05 M Na_2HPO_4 and 0.05 M NaH_2PO_4. The pH was adjusted using 0.5 M H_2SO_4 and 2 M NaOH.

Electrochemical measurements were carried out using a CHI 1205A computerized electrochemical workstation. The electrochemical cell had saturated Ag/AgCl as a reference electrode, platinum wire as a counter electrode and glassy carbon (area = 0.0798 cm^2) as a working electrode. Amperometric measurements were performed with an analytical rotator (AFMSRX, USA) connected with a rotating disc carbon electrode (electrode area = 0.24 cm^2). UV–visible spectra were recorded with a JASCO V770 and ^{1}H NMR spectra with a JEOL 300 MHz spectrometer. The morphological structure was characterized using scanning electron microscopy (SEM; Hitachi S-3000H), and elemental (energy-dispersive X-ray, EDX) analysis was carried out using a Horiba EMAX X-ACT (51-ADD0009) instrument. Electrochemical impedance spectroscopy (EIS) was carried out with a Zahner impedance instrument (Kroanch, Germany) from 0.1 Hz to 1 MHz frequency used for impedance analysis. Fourier transform infrared (FT-IR) spectra were recorded with a PerkinElmer spectrometer. Raman spectra were recorded using a Jobin Yvon T64000 spectrometer equipped with a charge coupled device detector cooled with liquid nitrogen. All the electrochemical experiments were carried out at ambient temperature.

2.2 | Synthesis of Pt-TPP

Pt-TPP was prepared using the method of Adler et al.[39] In brief, pyrrole (50 ml/0.8 M) was added into a refluxing flask, propionic acid (80 ml/0.8 M) was added and the mixture was refluxed for 45 min. The refluxed solution was cooled to room temperature, filtered and washed with methanol. After a hot water wash, purple crystals of TPP (90% yield) appeared (Scheme 1). The synthesized TPP (50 mg) was dissolved in chloroform (20 ml). Then, platinum(II) chloride (0.75 mmol) and benzonitrile were added into the TPP solution and refluxed. The reaction mixture was washed twice with water to remove excess unreacted materials. Finally, the solvent was removed using a rotatory evaporator. The resultant product of Pt-TPP (Scheme 2) was characterized and confirmed using ^{1}H NMR spectroscopy (Figures S1, S2) and UV–visible spectroscopy, and then stored in a refrigerator.[40]

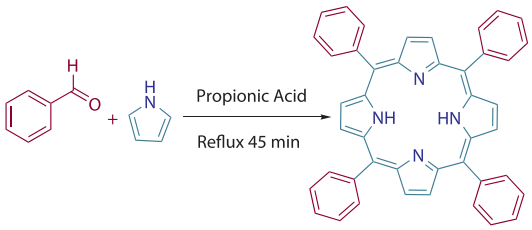

SCHEME 1 Synthesis of tetraphenylporphyrin (TPP)

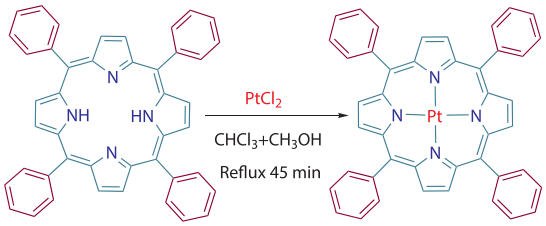

SCHEME 2 Synthesis of platinum tetraphenylporphyrin (Pt-TPP)

2.3 | Preparation of RGO/Pt-TPP Nanocomposite

Before electrode modification, a bare GCE was polished using alumina slurry then washed with anhydrous ethanol and distilled water followed by ultrasonication for 5 min. GO was prepared using a modified Hummer method.[41] The synthesized Pt-TPP was added (5 µl) into 2 ml of GO dispersion (1 mg ml^{-1}) and then the mixture was sonicated for 20 min for complete interaction between GO and Pt-TPP. The RGO/Pt-TPP nanocomposite (Scheme 3) was formed through π–π stacking interaction between Pt-TPP and RGO. A suspended solution (8 µl) of GO/Pt-TPP (S3) was drop-coated on the GCE surface and dried at room temperature. Then, the modified GCE was transferred into an electrochemical cell containing 0.05 M acetate buffer and a potential difference of 0 to −1.4 V was applied for GO reduction (S4). Finally, the RGO/Pt-TPP nanocomposite-modified GCE was obtained, and was stored in a refrigerator.

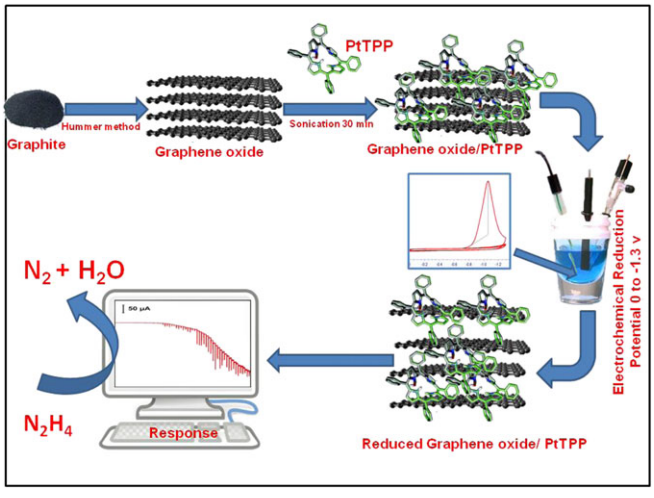

SCHEME 3 Preparation of RGO/Pt-TPP nanocomposite

3 | RESULTS AND DISCUSSION

3.1 | Characterization of nanocomposite

The ^{1}H NMR spectra of TPP and Pt-TPP are shown in Figures S1 and S2. ^{1}H NMR spectrum of TPP (300 MHz, $CDCl_3$, δ, ppm): 7.24 (s, 8H), 8.18 (d, 8H, J = 7.8 Hz), 7.75 (m, 12H), −2.81 (s, 2H). ^{1}H NMR spectrum of Pt-TPP (300 MHz, $CDCl_3$, δ, ppm): 7.74 (s, 8H), 8.19 (d, 8H, J = 5.4 Hz), 7.96 (m, 12H). The singlet N─H peaks (due to rapid exchange of the N─H protons) are found at very high field of −2.81 ppm (2H) because of shielding of the porphyrin ring. The disappearance of the NH proton signal in the spectrum of the Pt-TPP complex confirms the complete metallation between porphyrin and Pt.[42,43] The surface morphology of the as-prepared nanocomposite was examined using SEM. Figure 1 shows SEM images of GO, RGO, GO/Pt-TPP, Pt-TPP and RGO/Pt-TPP. The SEM image of GO displays a non-exfoliated sheet structure. The SEM image of RGO exhibits aggregated and exfoliated structure through the reduction of GO. In addition, the inset of Figure 1(C) shows a typical SEM image of as-synthesized Pt-TPP. The SEM image of GO/Pt-TPP clearly reveals that the Pt-TPP molecules are anchored on the GO surface. Furthermore, the SEM image of the RGO/Pt-TPP nanocomposite shows that the Pt-TPP molecules are uniformly distributed on the RGO surface via π–π stacking interaction and manipulates the uniform active surface area. The active surface area is used for electron transfer and electrocatalytic reaction. The inset of Figure 1(D) shows the EDX spectrum of the RGO/Pt-TPP nanocomposite, confirming the presence of C, N, O and Pt atoms in the composite.

Raman spectroscopy is widely used to characterize the crystal structure and disorder of graphene-based nanocomposites. The spectra show changes in the relative intensity of D and G bands.[44,45] The intensities of D and G bands are used to identify the functionalization of graphene-based nanomaterials.[46] Figure 2(A) shows the Raman spectra of

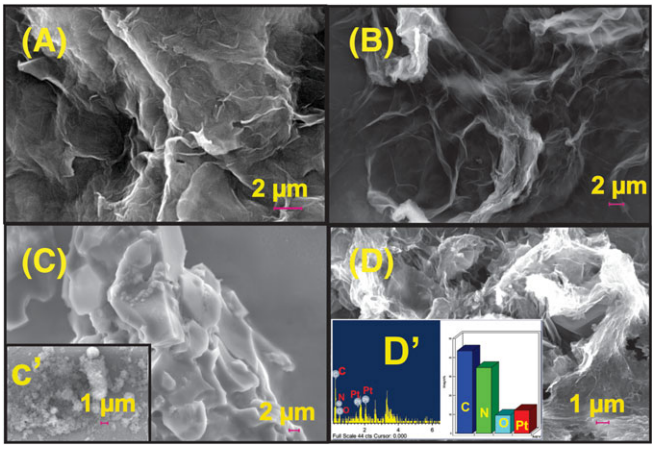

FIGURE 1 SEM images of (A) GO, (B) RGO, (C) GO/Pt-TPP and (D) RGO/Pt-TPP. Inset (C′) Pt-TPP; inset (D') EDX spectrum of RGO/Pt-TPP nanocomposite

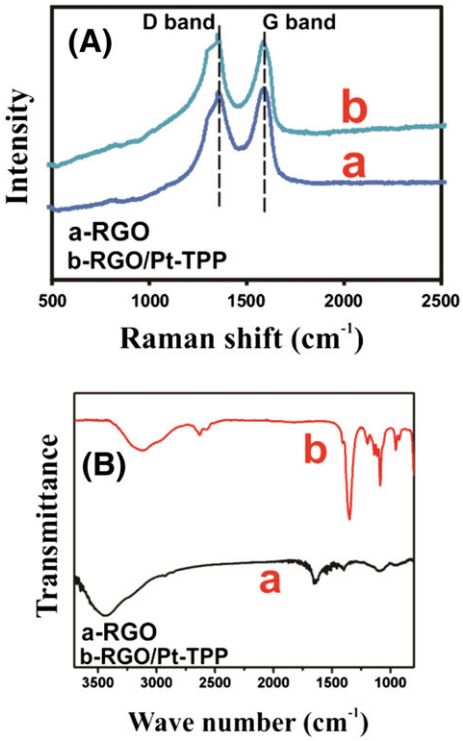

FIGURE 2 (A) Raman spectra of (a) RGO and (b) RGO/Pt-TPP nanocomposite. (B) FT-IR spectra of (a) RGO and (b) RGO/Pt-TPP nanocomposite

RGO and the RGO/Pt-TPP nanocomposite. The Raman spectrum of RGO exhibits two peaks at 1356 and 1592 cm^{-1} for D band and G band. The RGO/Pt-TPP nanocomposite spectrum shows the D band at 1347 cm^{-1} and the G band at 1597 cm^{-1}. The downshift of the D band and the upshift of the G band compared with RGO suggest a strong interaction between Pt-TPP and RGO.

FT-IR spectroscopy is an effective tool for identifying the functional groups in graphene-based nanomaterials. Figure S6 shows the FT-IR spectrum of GO and Figure 2(B) shows the FT-IR spectra of RGO and RGO/Pt-TPP. The FT-IR spectrum of GO exhibits sharp peaks at 3426, 1730, 1225 and 1063 cm^{-1} which are attributed to the stretching modes of ─OH, C═O, ─C─O (epoxy) and R─C─O (alkoxy), respectively. However, the intensities of these peaks are considerably reduced after the reduction of GO to RGO indicating the removal of oxygen functionalities and partial restoration of sp^2 network. The corresponding O─H stretching vibrations appear at 3400 cm^{-1}. Moreover, the C═O and C═C stretching vibrations are observed at 1720 and 1628 cm^{-1}, respectively. The peaks at 1285 and 1633 cm^{-1} are attributed to the C─N and C─C stretching vibrations. The symmetric and antisymmetric vibrations of ─CH_2 appear at 2933 and 2862 cm^{-1}. When Pt-TPP noncovalently interacts with RGO, positively shifted C═C and C═N bands of the RGO/Pt-TPP nanocomposite are obtained at 1668 and 1260 cm^{-1}.[28] The peaks at 3300 and 2925 cm^{-1} are assigned to N─H and C─H stretching vibrations. Therefore, the FT-IR spectra confirm the strong interaction between RGO and Pt-TPP.

Figure 3(A) shows the UV–visible spectra of GO, RGO, Pt-TPP, RGO/Pt-TPP and TPP. The UV–visible spectra were obtained at room temperature. GO and RGO show absorption bands at 290 and 296 nm, respectively. The RGO absorbance value is decreased compared to that of GO. The TPP spectrum shows an absorption peak of a Soret band at 418 nm and Q bands appear at 469, 514, 549, 590 and 647 nm. Moreover, the Pt-TPP spectrum shows the absorption peak of a Soret band at 415 nm and Q bands at 478, 520 and 523 nm. The Pt-TPP metallation is confirmed by decreasing of Soret band and Q bands as compared to TPP. The RGO/Pt-TPP nanocomposite spectrum exhibits a Soret band at 414 nm and Q bands at 468, 519 and 554 nm.[47] The red-shifting of the Soret band of RGO/Pt-TPP and decreasing intensity compared with Pt-TPP confirm the strong interaction between RGO and Pt-TPP.

The EIS plot shows two distinct regions: first, a semicircle region for electron transfer resistance (R_{ct}); second, a linear region for diffusion process. Figure 3(B) shows the EIS spectra of bare GCE, GCE/GO, GCE/GO/Pt-TPP, GCE/RGO and GCE/RGO/Pt-TPP in 5 mM $[FeCN_6]^{3-}$/$[FeCN_6]^{4-}$ solution containing 0.05 M PBS (pH = 7) with 0.1 M KCl electrolyte. The frequency range was fixed at 100 mHz to 100 kHz applied for impedance analysis. The R_{ct} value of each modified electrode can be identified by

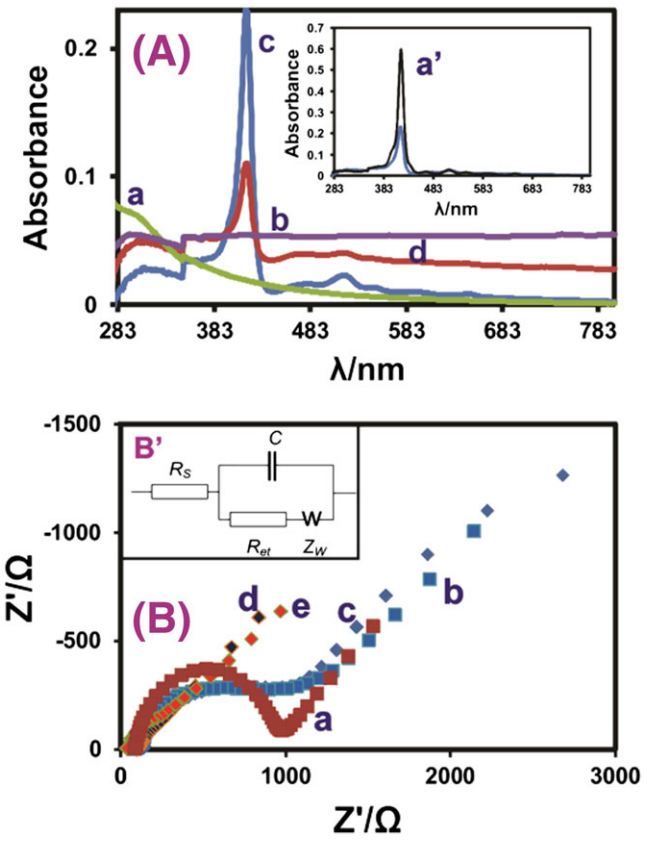

FIGURE 3 (A) UV–visible spectra of (a) GO, (b) RGO, (c) Pt-TPP and (d) RGO/Pt-TPP; inset (a') TPP. (B) EIS spectra of (a) bare GCE, (b) GCE/GO, (c) GCE/Pt-TPP, (d) GCE/RGO and (e) GCE/RGO/Pt-TPP in 0.1 M KCl containing 5 mM $[Fe(CN)_6]^{3-/4-}$

fitting the Nyquist plot with the Randle equivalent circuit model (Figure 3B'). The bare GCE shows a large semicircle with R_{ct} = 920 Ω, attributed to poor electron conductivity. Moreover, the GO-modified electrode shows a semicircle with R_{ct} of 706 Ω. On the other hand, GCE/Pt-TPP shows a semicircle with lower R_{ct} of 285 Ω compare to bare GCE and GO. This confirms that Pt-TPP enhances the electron transfer kinetics. In addition, GCE/RGO exhibits a small semicircle with R_{ct} of 191 Ω due to the large surface area increasing the electron transfer kinetics. Finally, GCE/RGO/Pt-TPP exhibits a depressed semicircle with electron transfer (R_{ct}) of 138 Ω, lower than that of the aforementioned modified electrodes due to the lower electrode resistance.

3.2 | Electrocatalytic oxidation at RGO/Pt-TPP nanocomposite-modified electrode

3.2.1 | Electro-oxidation of hydrazine at differently modified electrodes and for various concentrations

Figure 4(A) shows the cyclic voltammetry (CV) response for the electrocatalytic oxidation of hydrazine at differently modified electrodes, namely bare GCE, GCE/RGO, GCE/Pt-TPP, GCE/GO/Pt-TPP and GCE/RGO/Pt-TPP, in the presence of 200 μM hydrazine in nitrogen-saturated PBS (pH = 7) at a scan rate of 50 mV s^{-1}. The GCE/RGO/Pt-TPP modified electrode was also investigated in the absence of hydrazine in nitrogen-saturated PBS (pH = 7) at a scan rate of 50 mV s^{-1}. The CV curves of bare GCE and GCE/RGO show there is no response for the oxidation of hydrazine. The CV responses for GCE/Pt-TPP and GCE/GO/Pt-TPP exhibit hydrazine oxidation potential peak (E_p) at around 0.06 and 0.17 V and peak current (I_p) of 53.85 and 63.75 μA, respectively. The obtained CV curve of GCE/RGO/Pt-TPP shows higher I_p of 145.2 μA and lower E_p of −0.27 V. This reveals that GCE/RGO/Pt-TPP oxidizes hydrazine at a lower oxidation potential and higher oxidation peak current than all the other modified electrodes. This is due to the faster electron transfer kinetics owing to high surface area of RGO and better electrocatalytic activity of Pt-TPP. Fascinatingly, GCE/RGO/Pt-TPP acts as a better electrode material for the electrocatalytic oxidation of hydrazine than previously reported carbon nanomaterial-modified electrodes (Table 1). Figure 4(B) shows the CV curves of RGO/Pt-TPP nanocomposite-modified electrode for various concentrations of hydrazine in nitrogen-saturated PBS (pH = 7). With increasing concentration (0.5 to 5 μM) of hydrazine, the oxidation peak current increases linearly. This indicates that the modified electrode acts as a good electrode material for the oxidation of hydrazine without any electrode fouling.

3.2.2 | Effect of pH and scan rate on oxidation of hydrazine

The pH of the electrolyte is one of the crucial parameters that affect the electrocatalytic activity of hydrazine oxidation especially the peak potential of hydrazine. Figure 5(A) shows

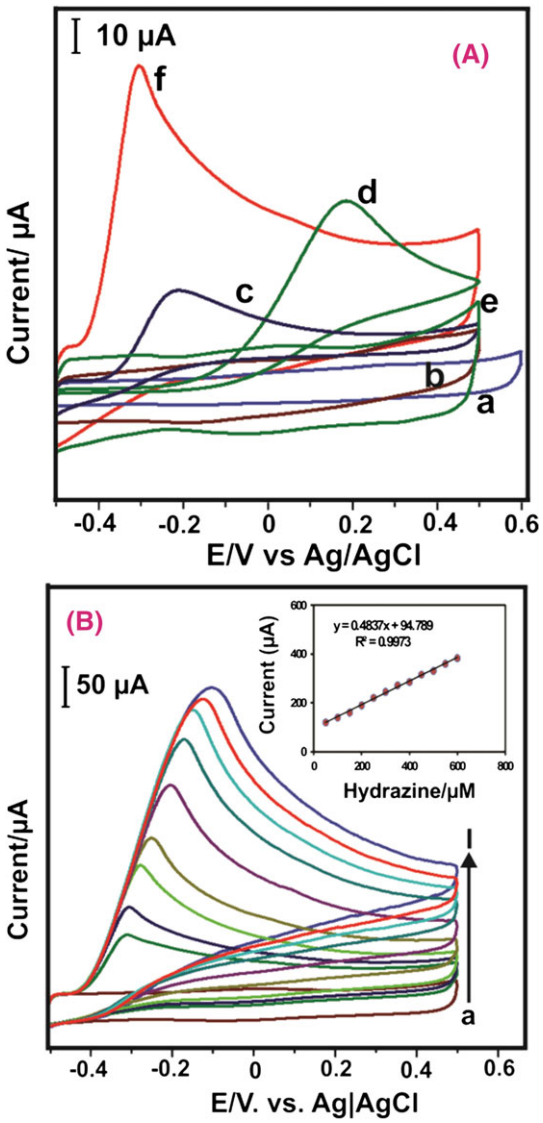

FIGURE 4 (A) CV response of (a) bare GCE, (b) GCE/RGO, (c) GCE/Pt-TPP, (d) GCE/GO/Pt-TPP and (f) GCE/RGO/Pt-TPP in presence of 200 μM hydrazine and (e) GCE/RGO/Pt-TPP in absence of hydrazine in nitrogen-saturated PBS (pH = 7) at a scan rate 50 mV s^{-1}. (B) CV response of RGO/Pt-TPP nanocomposite at various concentrations of hydrazine in 0.05 M PBS (pH = 7) at a scan rate 50 mV s^{-1}

the CV curves for pH varying from 3 to 11 at the RGO/Pt-TPP nanocomposite-modified electrode towards the oxidation of hydrazine (200 μM). A negative shift of E_p is observed with increasing pH and the peak current also markedly increases on varying the pH from 3 to 7 and thereafter peak current decreases. These results are explained by the fact that pK_a of hydrazine is 7.9. However, when the electrolyte pH is close to pK_a, hydrazine is in neutral form resulting in its facile oxidation. Hence, this leads to an increase the peak current of hydrazine at pH = 7. Figure 5(B) shows the linear relationship between pH and E_p. The obtained slope value of 54 mV/pH is very close to that of the theoretical Nernst equation which indicates that an equal number of protons and electrons transfer in the oxidation of hydrazine. Moreover, Figure 5(C) shows that the RGO/Pt-TPP

TABLE 1 Comparison of analytical performance of RGO/Pt-TPP nanocomposite with that of previously reported hydrazine sensors

Electrode material	LOD (μM)[a]	Linear range (μM)	Ref.
Cu/Cu_2O CNc[b]	0.022	0.25–800	[48]
(FeTsPc)[c]	0.0076	0.1–3	[7]
ZnO/Au Nps[d]	0.018	0.05–5	[49]
Rutin film/MWCNT[e]	0.61	2.0–190	[50]
Hematoxylin/MWCNT	0.68	2.0–122.8	[51]
CeNps[f]/mesoporous carbon	0.012	0.04–192	[52]
Graphene nanoflakes	0.3	0.5–7.5	[53]
Zinc oxide nanonail	0.2	0.1–1.2	[18]
(PdNPs[g]–EDAC[h]/GCE[i])	1.5	5–150	[54]
PEG[j]/CdS Nps[k]//Au electrode[l]	0.061	0.1–1	[55]
RGO[m]/Pt-TPP Nc[n]	0.005	0.013–232	This work

[a]Limit of detection.

[b]Carbon nanocomposite.

[c]Iron tetra-sulfonated phthalocyanine.

[d]Gold nanoparticles.

[e]Multiwalled carbon nanotube.

[f]Cerium nanoparticles.

[g]Palladium nanoparticles.

[h]Ethylenediamine cellulose.

[i]Glassy carbon electrode.

[j]Poly(ethylene glycol).

[k]Cadmium sulfide nanoparticle.

[l]Gold electrode.

[m]Reduced graphene oxide.

[n]Platinum tetraphenylporphyrin.

nanocomposite-modified electrode has the highest I_p at pH = 7; therefore we chose neutral pH (7) for all the electrochemical experiments.

Figure 6 shows the effect of scan rate on the RGO/Pt-TPP nanocomposite-modified electrode in the presence of 200 μM hydrazine in PBS (pH = 7). The peak current increases linearly with increasing scan rate (10 to 100 mV s^{-1}). In addition, the anodic peak potential shifts to a more positive value as scan rate is increased. The inset of Figure 6 shows a plot of the square root of scan rate ($\nu^{1/2}$) against anodic peak current (I_p), exhibiting a linear relationship, indicating that the hydrazine oxidation reaction at the RGO/Pt-TPP nanocomposite-modified electrode is a diffusion-controlled electron transfer process. The corresponding linear regression equation can be expressed as $I_p = 287.5\nu^{1/2}–26.6$ (where I_p is in μA and ν in V s^{-1}), for which $R^2 = 0.9925$. A plot (Figure S6) of anodic peak potential E_{pa} versus log ν exhibits a linear relation. Therefore, the electrocatalytic oxidation of hydrazine at the RGO/Pt-TPP nanocomposite-modified electrode is an electrochemically irreversible process. The corresponding linear regression equation can be expressed as E_{pa} (V) = 0.115 log ν + 0.3194. E_{pa} can be represented by a Tafel equation based on the following:[56]

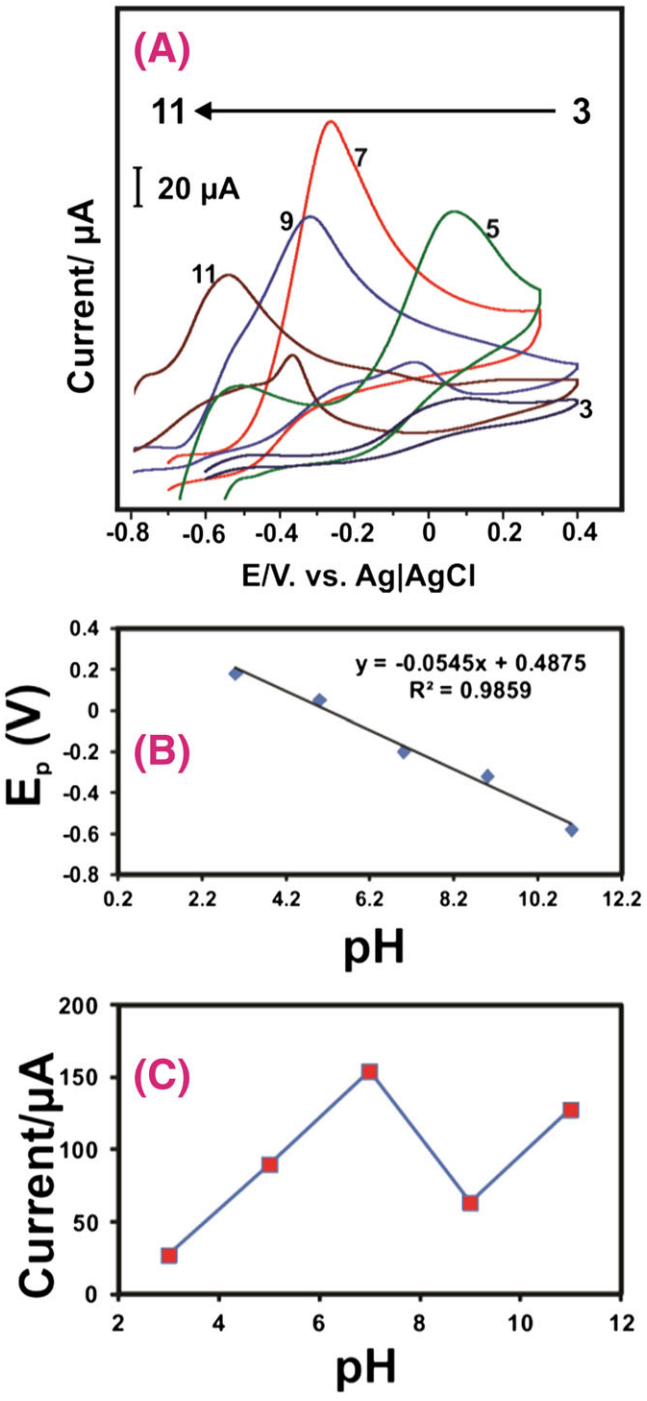

FIGURE 5 (A) CV response of RGO/Pt-TPP nanocomposite-modified GCE in 200 μM hydrazine-containing solutions with various pH (3, 5, 7, 9 and 11) at a scan rate of 50 mV s^{-1}. (B) Calibration plot for pH versus E_p. (C) Calibration plot for pH versus I_p

$$E_{pa} = \left[\frac{2.303RT}{(1-\alpha)n_aF}\right] \log\nu + K \quad (1)$$

where R, T and F are constant values (R = 8.314 J K^{-1} mol^{-1}, T = 298 K and F = 96 485 C mol^{-1}), α is the electron transfer coefficient, n_a is the number of electron transfers involved in the rate-determining step and K is a constant. Furthermore, an electron transfer of the

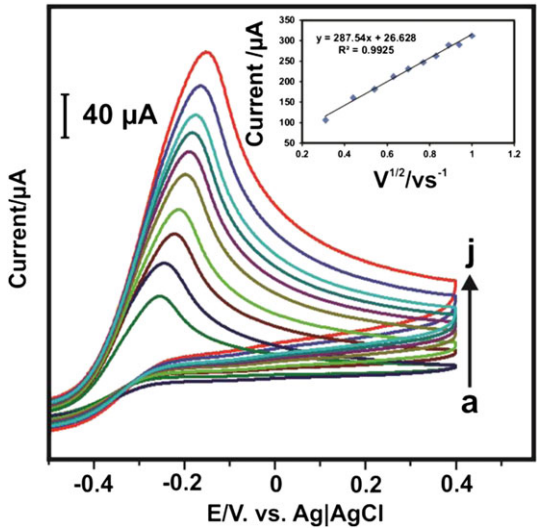

FIGURE 6 CV response of RGO/Pt-TPP nanocomposite-modified GCE in PBS containing 200 μM hydrazine at various scan rates (10 to 100 mV s^{-1}). Inset: calibration plot of square root of scan rate versus peak current

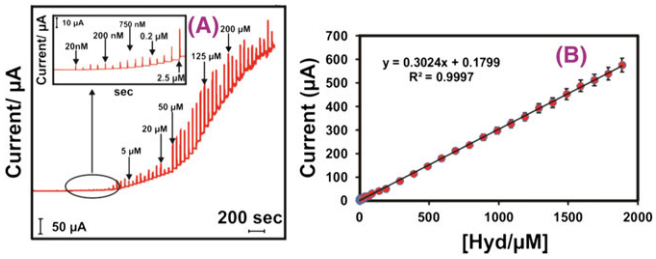

FIGURE 7 (A) Amperometric response (E_{app} = −0.25 V) for oxidation of hydrazine with various concentrations in PBS (pH = 7) at RGO/Pt-TPP nanocomposite-modified electrode. (B) Peak current versus hydrazine concentration

overall reaction was calculated using the following equation:

$$I_p = \left(2.99\times10^5\right)n[(1-\alpha)n_a]^{1/2}AC_0D_0^{1/2}v^{1/2} \quad (2)$$

where A is the electrode area, D_0 is the diffusion coefficient and C_0 is the bulk concentration of hydrazine. Hence, substituting all the values in equation 2, the value of n is estimated to be 4. The oxidation of hydrazine at the RGO/Pt-TPP nanocomposite-modified electrode involves four electron transfers, which can be expressed as

$$N_2H_4+H_2O\rightarrow N_2H_3+H_3O+e^-(\text{slow}) \quad (3)$$

$$N_2H_3+3H_2O\rightarrow N_2+3H_3O+3e^-(\text{fast}) \quad (4)$$

Here, equation 3 is a slow, one-electron transfer and the rate-determining step. The second step, equation 4, is a fast three-electron transfer reaction. Thus, the overall hydrazine electron transfer reaction can be summarized as follows:[57]

$$N_2H_4+4H_2O\rightarrow N_2+4H_3O+4e^- \quad (5)$$

3.3 | Amperometric Determination of Hydrazine

The amperometric method is more sensitive, of higher precision and involves lower background current than other voltammetric methods.[58] A calibration curve was used for determining the limit of detection (LOD), linear range and sensitivity of the modified electrode. Figure 7(A) shows the amperometric response of RGO/Pt-TPP nanocomposite-modified rotating disc electrode upon each successive addition of various concentrations of hydrazine into continuously stirred nitrogen-saturated PBS at a rotation speed of 2500 rpm and the applied potential being held at −0.25 V. The sensor exhibits a sharp amperometric response for each addition of hydrazine with regular time interval (50 s). The steady-state current response of hydrazine is reached within 3 s at the RGO/Pt-TPP nanocomposite-modified electrode, indicating a fast response of the oxidation of hydrazine. Figure 7(B) shows the calibration plot between the hydrazine concentration and current response. The corresponding linear regression equation is expressed as I_p (A) = 0.3024 × [hydrazine (μM)] + 0.1799. The sensitivity of the sensor is estimated to be 1.44 μA μM^{-1} cm^{-2} from the slope values. Moreover, the LOD is calculated to be 5 nM (LOD = 3*Sb*/*S*, where *Sb* is the standard deviation of the signal and *S* the slope value). Notably, the prepared sensor exhibits a linear response from 13 nM to 232 μM. This indicates the outstanding electrocatalytic oxidation of hydrazine at the RGO/Pt-TPP nanocomposite-modified electrode. In addition, based on the above results we conclude that Pt-TPP plays a vital role for the oxidation of hydrazine due to good electron transfer properties and homogeneous electron-rich environment. Moreover, Pt-TPP considerably reduces the overpotential of hydrazine oxidation which is advantageous for avoiding interferences and leading to less power consumption. In addition, the high surface area of RGO provides more active sites for the interaction with Pt-TPP, which makes the composite highly suitable for electrocatalytic reaction. Also, the good synergic effect between RGO and Pt-TPP plays a significant role in enhancing the electrocatalysis of hydrazine.[36,38] As a result, the performance of the RGO/Pt-TPP nanocomposite sensor towards hydrazine is significantly better than that of several previously reported graphene nanocomposite-based modified electrodes.

3.4 | Interference and real sample analysis

The selectivity of the RGO/Pt-TPP nanocomposite-modified electrode was investigated using the amperometric method. Figure 8 shows the amperometric response of anions, cations and biological molecules. It is very important to evaluate the response of these kinds of interfering ions,

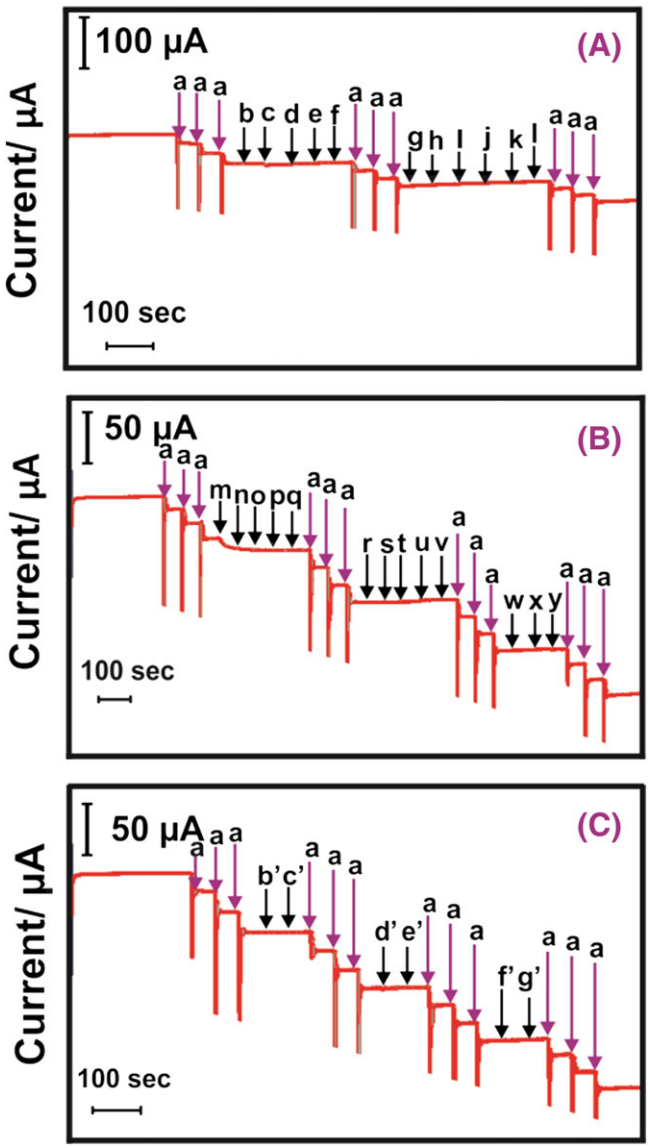

FIGURE 8 Amperometric response ($E_{app} = -0.25$ V) of hydrazine at RGO/Pt-TPP nanocomposite-modified electrode in the presence of common interference ions. (A) Addition of (a) 1 µM hydrazine and 500 µM addition of anions (b) Br^-, (c) I^-, (d) Cl^-, (e) NO_3^-, (f) F^-, (g) SO_4^-, (h) S_2^-, (i) HCO_3^-, (j) $H_2PO_4^-$, (k) SO_3^{2-}, (l) BrO_3^-; (B) cations (m) Cu^{2+}, (n) Zn^{2+}, (o) Cr^{2+}, (p) Sr^{2+}, (q) K^+, (r) Sn^{2+}, (s) Ti^{4+}, (t) Ba^{2+}, (u) NH^{4+}, (v) Ca^{2+}, (w) Mg^{2+}, (x) Zr^{2+}, (y) Hg^{2+}; (C) biological interference samples (b') dopamine, (c') glucose, (d') fructose, (e') lactose, (f') arginine, (g') ascorbic acid

because they are commonly present in various types of contaminated water. The amperometric response of the RGO/Pt-TPP nanocomposite-modified electrode was evaluated for the addition of 1 µM hydrazine, addition of 500 µM anions and cations and addition of biological interferences. The RGO/Pt-TPP nanocomposite-modified electrode exhibits a good response only for each addition of hydrazine. Interestingly, there is no response apparent even for 500-fold excess addition of the common interfering ions. Therefore, the RGO/Pt-TPP nanocomposite has excellent selectivity for the determination of hydrazine in the presence of common interfering ions. The practicability of the modified sensor towards determination of hydrazine in spiked water samples was investigated (Table 2). The fabricated sensor acquires acceptable recoveries from the various water samples, and it is evident that the RGO/Pt-TPP nanocomposite-modified electrode has practical feasibility of the determination of hydrazine.

TABLE 2 Determination of hydrazine in ground water samples using RGO/Pt-TPP nanocomposite-modified GCE

Sample	Added (µM)	Found (µM)	Recovery (%)	RSD (%)[a]
River water	100, 200	103.2, 198.3	103.2, 99.1	3.43.7
Sea water	100, 200	101.5, 202.4	101.5, 101.2	2.82.6
Rain water	100, 200	101.5, 199.2	101.5, 99.6	3.22.9

[a]Relative standard deviation of three individual measurements.

3.5 | Repeatability, reproducibility and stability studies

Repeatability, reproducibility and storage stability of the proposed RGO/Pt-TPP nanocomposite-modified electrode were investigated using CV in nitrogen-saturated PBS containing 0.1 mM hydrazine at a scan rate 50 mV s^{-1}. The proposed sensor material exhibits an acceptable repeatability with relative standard deviation of 2.16% for 10 repeat measurements examined using a single modified electrode (Figure S7). Moreover, the sensor shows appreciable reproducibility of 2.98% for six individual measurements carried out using six individual modified electrodes (Figure S7). The storage stability of the RGO/Pt-TPP nanocomposite-modified electrode towards oxidation of 0.1 mM hydrazine was monitored every day. The electrode was stored in PBS (pH = 7) at 4 °C when not in use. Furthermore, during the four-week storage period the modified electrode exhibited good catalytic response towards the detection of hydrazine without any peak current and potential changes. Remarkably, 96.62% of the initial peak current (I_p) was retained after continuous usage; this shows the good storage stability of the proposed sensor (Figure S9). Figure 9 shows the operational stability of the RGO/Pt-TPP nanocomposite-modified electrode investigated using the amperometry method. The stability study was carried out for up to 4000 s with the experimental conditions similar to those described above. The sensor retains 97.6% of its initial current response after a continuous run for up to 4000 s in

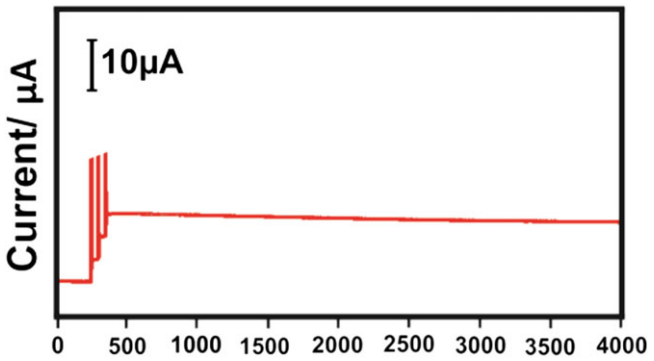

FIGURE 9 Amperometric stability studies of RGO/Pt-TPP nanocomposite

200 μM hydrazine-containing PBS. The results indicate the excellent operational stability of the RGO/Pt-TPP nanocomposite.

4 | CONCLUSIONS

In summary, we have successfully prepared a RGO/Pt-TPP nanocomposite using noncovalent π–π interaction. The prepared nanocomposite was confirmed using SEM and UV, FT-IR and Raman spectroscopies. Electrochemical studies were carried out using CV and the amperometric method. The modified sensor exhibited a wide linear range from 13 nM to 232 μM with high sensitivity of 1.44 μA μM^{-1} cm^{-2} and LOD of 5 nM. Moreover, the sensor performed well even in the presence of 500-fold excess concentration of interfering molecules and ions. The practical feasibility of the sensor was confirmed by determination of hydrazine in ground water samples with good recoveries. The fabricated sensor exhibited acceptable selectivity, stability, repeatability and reproducibility. The excellent electrocatalytic activity of the RGO/Pt-TPP nanocomposite means that it can be explored as an outstanding electrode material for the detection of hydrazine.

ACKNOWLEDGMENTS

The authors extend their appreciation to the International Scientific Partnership Program ISPP at King Saud University for funding this research work through ISPP#6. This project was also supported by the National Science Council and Ministry of Science and Technology, Taiwan (ROC).

REFERENCES

[1] R. Devasenathipathi, V. Mani, S. M. Chen, D. Arulraj, V. S. Vasantha, *Electrochim. Acta* **2014**, *135*, 260.

[2] S. Dutta, C. Ray, S. Mallick, S. Sarkar, A. Roy, T. Pal, *RSC Adv.* **2015**, *5*, 51690.

[3] J. Li, H. Xie, L. Chen, *Sens. Actuators B* **2011a**, *153*, 239.

[4] C. A. Pessoa, Y. Gushikem, S. Nakagaki, *Electroanalysis* **2002**, *14*, 15.

[5] Y. You, Y. Yang, Z. Yang, *J. Solid State Electrochem.* **2013**, *17*, 701.

[6] Z. Zhao, Y. Sun, P. Li, S. Sang, W. Zhang, J. Hu, K. Lian, *J. Electrochem. Soc.* **2014**, *161*, 157.

[7] R. Devasenathipathy, S. Palanisamy, S. M. Chen, C. Karuppiah, V. Mani, S. K. Ramaraj, M. A. Ali, F. M. A. A. Hemaid, *Electroanalysis* **2015**, *27*, 1403.

[8] US Environmental Protection Agency, Integrated risk information system (IRIS) on hydrazine/hydrazine sulfate, National Center for Environmental Assessment, Office of Research and Development, Washington, DC, **1999**.

[9] A. Safavi, M. A. Karimi, *Talanta* **2002**, *58*, 785.

[10] G. W. Watt, J. D. Chrisp, *J. Anal. Chem.* **1952**, *24*, 2006.

[11] J. Budkuley, *Microchim. Acta* **1992**, *108*, 103.

[12] S. Ikeda, H. Satake, Y. Kohri, *Chem. Lett.* **1984**, *13*, 873.

[13] M. Sun, L. Bai, D. Q. Liu, *J. Pharm. Biomed. Anal.* **2009**, *49*, 529.

[14] M. A. Koupparis, T. P. Hadjiioannou, *Talanta* **1978**, *25*, 477.

[15] A. M. Eibrashy, L. A. E. Hussein, *Anal. Lett.* **1997**, *30*, 609.

[16] W. Siangproh, O. Chailapakul, R. Laocharoensuk, J. Wang, *Talanta* **2005**, *67*, 903.

[17] J. P. Liu, Y. Y. Li, J. Jiang, X. T. Huang, *Dalton Trans.* **2010**, *39*, 8693.

[18] A. Umar, M. M. Rahman, S. H. Kim, Y. B. Hahn, *Chem. Commun.* **2008**, *166*.

[19] J. Wang, Z. Lu, *Electroanalysis* **1989**, *1*, 517.

[20] A. Krittayavathananon, P. Srimuk, S. Luanwuthi, M. Sawangphruk, *Anal. Chem.* **2014**, *86*, 12272.

[21] S. Park, J. An, J. R. Potts, A. Velamakanni, S. Murali, R. S. Ruoff, *Carbon* **2011**, *49*, 3019.

[22] J. Ping, Y. Wang, Y. Ying, J. Wu, *Anal. Chem.* **2012**, *84*, 3473.

[23] J. T. Robinson, F. K. Perkins, E. S. Snow, Z. Wei, P. E. Sheehan, *Nano Lett.* **2008**, *10*, 3137.

[24] P. D. Beer, M. G. B. Drew, R. J. Jagessar, *Dalton Trans.* **1997**, *881*.

[25] M. Biesaga, K. Pyrzynska, M. Trojanowicz, *Talanta* **2000**, *51*, 209.

[26] J. E. Falk, *Porphyrins and Metalloporphyrins*, Elsevier, New York **1975**.

[27] A. Takai, C. P. Gros, J. M. Barbe, R. Guilard, S. Fukuzumi, *Chem. – Eur. J.* **2009**, *15*, 3110.

[28] L. Zheng, D. Ye, L. Xiong, J. Xu, K. Tao, Z. Zou, D. Huang, X. Kang, S. Yang, J. Xia, *Anal. Chim. Acta* **2013**, *768*, 69.

[29] S. K. Lee, I. Okura, *Anal. Commun.* **1997a**, *34*, 185.

[30] S. K. Lee, I. Okura, *Anal. Chim. Acta* **1997b**, *342*, 181.

[31] R. R. D. Haas, R. P. M. V. Gijlswijk, E. B. Vandertol, J. M. A. A. Zijlmans, T. B. Schut, J. Bonnet, N. P. Verwoerd, H. J. Tanke, *J. Histochem. Cytochem.* **1997**, *45*, 1279.

[32] H. Kunkely, A. Vogler, *Inorg. Chim. Acta* **1997**, *254*, 417.

[33] H. Brunner, K. M. Schellerer, B. Treittinger, *Inorg. Chim. Acta* **1997**, *264*, 67.

[34] A. Ferri, G. Polzonetti, S. Licoccia, R. Paolesse, D. Favretto, P. Traldi, M. V. Russo, *Dalton Trans.* **1998**, *4063*.

[35] H. Yuan, L. Thomas, L. K. Woo, *Inorg. Chem.* **1996**, *35*, 2808.

[36] H. P. Li, B. Zhou, Y. Lin, L. R. Gu, W. Wang, K. A. S. Fernando, S. Kumar, L. F. Allard, Y. P. Sun, *J. Am. Chem. Soc.* **2004**, *126*, 1014.

[37] G. M. A. Rahman, D. M. Guldi, S. Campidelli, M. Prato, *J. Mater. Chem.* **2006**, *16*, 62.

[38] W. Zhang, A. U. Shaikh, E. Y. Tsui, T. M. Swager, *Chem. Mater.* **2009**, *21*, 3234.

[39] A. D. Adler, F. R. Longo, J. D. Finarelli, J. Goldmacher, J. Assour, L. Korsakoff, *J. Org. Chem.* **1967**, *32*, 476.

[40] G. H. Barnett, M. F. Hudson, K. M. Smith, *J. Chem. Soc.* **1975**, *14*, 1401.

[41] W. S. Hummers, R. E. Offeman, *J. Am. Chem. Soc.* **1958**, *80*, 1339.

[42] C. He, Q. He, C. Deng, L. Shi, D. Zhu, Y. Fu, H. Cao, *Chem. Commun.* **2010**, *46*, 7536.

[43] J. R. Sommer, A. H. Shelton, A. Parthasarathy, I. Ghiviriga, J. R. Reynolds, K. S. Schanze, *Chem. Mater.* **2011**, *23*, 5296.

[44] Y. Guoa, X. Suna, Y. Liua, W. Wangb, H. Qiua, J. Gao, *Carbon* **2012**, *50*, 2513.

[45] A. Jorio, R. Saito, G. Dresselhaus, M. S. Dresselhaus, *Raman Spectroscopy in Graphene Related Systems*, Wiley-VCH, Weinheim **2011**.

[46] A. C. Ferrari, J. Robertson, *Phys. Rev. B* **2000**, *61*, 14095.

[47] P. Chen, O. S. Finikova, Z. Ou, S. A. Vinogradov, K. M. Kadish, *Inorg. Chem.* **2012**, *51*, 6200.

[48] Z. Zhao, Y. Wang, P. Li, S. Sang, W. Zhang, J. Hu, K. Lian, *Anal. Methods* **2015**, *7*, 9040.

[49] R. Madhu, B. Dinesh, S. M. Chen, R. Saraswathi, V. Mani, *RSC Adv.* **2015**, *5* .54379

[50] H. R. Zare, Z. Sobhani, M. M. Ardakani, *J. Solid State Electrochem.* **2007**, *11*, 971.

[51] H. R. Zare, N. Nasirizadeh, *Electrochim. Acta* **2007**, *52*, 4153.

[52] Y. Liu, Y. Li, X. He, *Anal. Chim. Acta* **2014**, *819*, 26.

[53] S. Mutyala, J. Mathiyarasu, *Sens. Actuators, B* **2015**, *210*, 692.

[54] H. Ahmar, S. Keshipour, H. Hosseini, A. R. Fakhari, A. Shaabani, A. Bagheri, *J. Electroanal. Chem.* **2013**, *690*, 96.

[55] K. Khushboo, A. Umar, S. K. Kansal, S. K. Mehta, *Sens. Actuators. B.* **2013**, *188*, 372.

[56] N. Li, M. Zhu, M. Qu, X. Gao, X. Li, W. Zhang, J. Zhang, J. Ye, *J. Electroanal. Chem.* **2011b**, *651*, 12.

[57] H. M. Nassef, A. E. Radi, C. K. O'Sullivan, *J. Electroanal. Chem.* **2006**, *592*, 139.

[58] S. Palanisamy, B. Thirumalraj, S. M. Chen, *RSC Adv.* **2015**, *5* .94591

SUPPORTING INFORMATION

Additional Supporting Information may be found online in the supporting information tab for this article.

How to cite this article: Sakthinathan S, Kubendhiran S, Chen S-M, Govindasamy M, Al-Hemaid FMA, Ajmal Ali M, Tamizhdurai P, Sivasanker S. Metallated porphyrin noncovalent interaction with reduced graphene oxide-modified electrode for amperometric detection of environmental pollutant hydrazine. *Appl Organometal Chem*. 2017; e3703. doi: 10.1002/aoc.3703